

1 Development of a new gas flaring emission data set for southern West Africa

2
3 Konrad Deetz and Bernhard Vogel

4
5 Institute of Meteorology and Climate Research, Karlsruhe Institute of Technology (KIT), Karlsruhe, Germany

6
7 Correspondence to: Konrad Deetz (konrad.deetz@kit.edu)

8 9 HIGHLIGHTS

- 10
11 - Development of a new gas flaring emission parameterization for air pollution modeling.
12 - Combination of remote sensing observation and physical based combustion calculation.
13 - Application to the significant gas flaring region southern West Africa.
14 - Comprehensive assessing of the parameterization uncertainties.
15 - Comparison with existing gas flaring emission inventories.

16 17 Keywords:

18
19 Gas flaring
20 Emission parameterization
21 Emission uncertainty
22 Pollution modeling
23 Carbon dioxide

24 25 ABSTRACT

26
27 A new gas flaring emission parameterization has been developed which combines remote sensing
28 observations using VIIRS nighttime data with combustion equations. The parameterization has been
29 applied to southern West Africa, including the Niger Delta as a region which is highly exposed to gas
30 flaring. Two two-month datasets for June-July 2014 and 2015 were created. The parameterization
31 delivers emissions of CO, CO₂, NO, NO₂ and SO₂. A flaring climatology for both time periods has been
32 derived. The uncertainties owing to cloud cover, parameter selection, natural gas composition and
33 the interannual differences are assessed. Largest uncertainties in the emission estimation are linked
34 to the parameter selection. It can be shown that the flaring emissions in Nigeria have significantly
35 decreased by 25% from 2014 to 2015. Existing emission inventories were used for validation. CO₂
36 emissions with the estimated uncertainty in brackets of 2.7 (^{3.6}/_{0.5}) Tg y⁻¹ for 2014 and 2.0 (^{2.7}/_{0.4}) Tg
37 y⁻¹ for 2015 were derived. Regarding the uncertainty range, the emission estimate is in the same
38 order of magnitude compared to existing emission inventories with a tendency for underestimation.
39 The deviations might be attributed to a shortage in information about the combustion efficiency
40 within southern West Africa, the decreasing trend in gas flaring or inconsistent emission sector
41 definitions. The parameterization source code is available as a package of R scripts.

42 43 1. Introduction

44
45 Gas flaring is a globally used method to dispose flammable, toxic or corrosive vapors to less reactive
46 compounds at oil production sites and refineries. In regions of insufficient transportation
47 infrastructure or missing consumers, flaring is also commonly applied.

48 CDIAC (2015a) estimated the global gas flaring emission of carbon dioxide to 267.7 million tons
49 (0.83% of total emissions) in 2008. Flaring and venting of gas significantly contributes to the
50 greenhouse gas emissions and therefore to the global climate change. The five countries with the
51 highest flaring amount in billion cubic meters (bcm) are Russia (35), Nigeria (15), Iran (10), Iraq (10)
52 and USA (5) (World Bank, 2012). These estimates were produced by National Oceanic and
53 Atmospheric Administration (NOAA) using Defense Meteorological Satellite Program (DMSP) remote
54 sensing data. Preliminary updates in global flaring estimates from NOAA for 2013 and 2014 are
55 available at http://ngdc.noaa.gov/eog/viirs/download_global_flare.html.

56 In recent time, especially with the development of remote sensing observation techniques (e.g.
57 Elvidge et al. (1997, 2013)), emissions from gas flaring moved in the focus of atmospheric research
58 involving the efforts in reducing the pollution and the waste of resources. The World Bank led the
59 initiatives “Global Gas Flaring Reduction Partnership” (GGFR) and “Zero Routine Flaring by 2030” to
60 promote the efficient use of flare gas.

61 Instead of relying on national statistics of gas production and consumption for estimating the flaring
62 amount, remote sensing techniques can estimate the flaring amount directly via multispectral data
63 (Elvidge et al., 2013). Elvidge et al. (2009) developed a 15 year dataset of global and national gas
64 flaring efficiency from 1994 to 2008 by using data from DMSP. Elvidge et al. (2015) presented
65 methods to derive global surveys of natural gas flaring using DMSP. For 2012 they have identified
66 7467 flares globally, with an estimated volume of flared gas of 143 (± 13.6) bcm. Doumbia et al.
67 (2014) combined DMSP with emission factors for flaring, to estimate the flaring emissions for SWA.
68 The satellite product Visible Infrared Imaging Radiometer Suite (VIIRS) Nightfire (Elvidge et al., 2013),
69 which is free available as “VIIRS Nightfire Nighttime Detection and Characterization of Combustion
70 Sources” (VIIRS, 2015a) (VNF hereafter), is now the most widely used product to derive flaring
71 emissions from satellite imagery. By using VNF, Zhang et al. (2015) estimated the methane
72 consumption and the release of CO₂ from gas flaring for the northern U.S. which agree with field data
73 within an uncertainty range of $\pm 50\%$.

74 Also in the second largest flaring country Nigeria, the awareness of gas flaring increases. Nigeria
75 shows the fourth highest number of flare sites (approx. 300) worldwide after USA, Russia and Canada
76 (Elvidge et al., 2015). On gasflaretracker.ng the attention of the government, industry and society is
77 called to the flaring problem by interactive maps of flare infrastructure, amounts and costs. The
78 implications of gas flaring in Nigeria are far-reaching. It influences the environment by noise and
79 deterioration of the air quality (Osuji and Avwiri, 2005). Nwankwo and Ogagarue (2011) have
80 measured higher concentrations of heavy metals in surface water of a gas flared environment in
81 Delta State Nigeria. Adverse ecological and bacterial spectrum modifications by gas flaring are
82 indicated by Nwaugo et al. (2006). Gas flaring also causes acid rain which causes economic burden
83 via rapid corrosion of zinc roofs (Ekpoh and Obia, 2010) and causes retardation in crop growth owing
84 to high temperatures (Dung et al., 2008).

85 The project DACCIWA (Dynamics-aerosol-chemistry-cloud interactions in West Africa, Knippertz et al.
86 (2015)) investigates the influence of anthropogenic and natural emissions on the atmospheric
87 composition over SWA, including the flaring hotspot Nigeria, to quantify the effects on meteorology
88 and cloud characteristics. To consider the SWA gas flaring emissions (e.g. in an atmospheric model),
89 this study presents a method to derive emission fluxes by combining the state of the art flaring
90 detection VNF and the combustion equations of Ismail and Umukoro (2014) which does not use
91 emission factors. The new parameterization is robust and easy to apply to new research questions
92 according flexibility in the spatiotemporal resolution.

93 The parameterization is presented in Section 2. Results of the application to SWA, including the
94 spatial distribution of gas flaring, the emission estimation and the uncertainty assessment are
95 investigated in Section 3. Section 4 places the emission estimates in the context of existing
96 inventories. The results are summarized and discussed in Section 5.

97

98 **2. Parameterization of gas flaring emissions**

99

100 The new parameterization for gas flaring presented here, is based on VIIRS Nightfire Nighttime
101 Detection and Characterization of Combustion Sources (VNF hereafter) and the combustion
102 equations of Ismail and Umukoro (2014) (IU14 hereafter).

103

104 **2.1 Remote sensing identification of gas flares**

105

106 VIIRS (Visible Infrared Imaging Radiometer Suite) is a scanning radiometer for visible and infrared
107 light on board the sun-synchronous Suomi National Polar-orbiting Partnership weather satellite
108 (Suomi-NPP) (NASA, 2016). It can detect combustion sources at night (e.g. bush fires or gas flares) by
109 spectral band M10. To confirm these sources and to eliminate noise, the Day/Night Band (DNB), M7,
110 M8 and M12 are used in addition. By fitting these measured spectra to the Planck radiation curve,
111 background and source temperatures can be deduced (VIIRS, 2015a).

112 The data is freely available as daily cloud corrected data from March 2014 to present. The files
113 include among others the location of the combustion sources, source temperature T_s , radiant heat H
114 and time of observation. VNF does not distinguish between the different combustion sources (e.g.
115 wild fires or flaring). To extract the flaring information from VNF a postprocessing is necessary. For
116 this study we have decided for a two month period of observation. This allows a compilation of a
117 flaring climatology in terms of the locations and emissions and a robust estimation of uncertainty
118 owing to cloud coverage and parameters that have to be prescribed for IU14. We have selected the
119 month June and July because the gas flaring emission dataset will be used within the regional online-
120 coupled chemistry model COSMO-ART (Vogel et al., 2009) during the measurement campaign of the
121 project DACCIWA, which took place in June/July 2016. This campaign includes airborne, ground
122 based and remote sensing observations of meteorological conditions and air pollution
123 characteristics. COSMO-ART is one of the forecasting models of the DACCIWA campaign and delivers
124 spatiotemporal aerosol/chemistry distributions. The data for June/July 2014 and June/July 2015 are
125 used to allow also for an interannual comparison and to assess the uncertainty owing to changes in
126 flare processes (e.g. built-up or dismantling, increase or decrease in combustion). The dataset
127 includes the countries which can affect SWA with their flaring emissions, in particular Ivory Coast,
128 Ghana, Nigeria, Cameroon, Gabon, Congo, the Democratic Republic of the Congo and Angola. The
129 extraction of the flaring information from the VNF data (VNF_{flare} hereafter) was realized by the Earth
130 Observation Group of NOAA. Within VNF_{flare} a csv file for every SWA flare is available, containing the
131 flaring history in June/July 2014 and 2015. For this study we use the location, source temperature
132 and radiant heat.

133

134 **2.2 Emission estimation method**

135

136 The principle emission estimation methodology used in this study follows IU14. The gas flaring
137 emissions are estimated based on combustion equations for incomplete combustion including six
138 flaring conditions given in Tab. 1. The equations are introduced in detail in IU14 and are therefore

139 not presented here. This section concentrates on the application of the method of IU14 to the
 140 VNF_{flare} data and the research domain SWA.

141
 142 **Tab.1.** Reaction types for incomplete combustion of flared gas, depending on availability of sulfur in the flared gas and the
 143 temperature in the combustion zone which determines the formation of NO and NO₂.
 144

Reaction type	Sulfur in flared gas	Source temperature (K)	NO _x formation
1	No	< 1200	no
2	Yes	< 1200	no
3	No	$1200 \leq T_s \leq 1600$	only NO
4	Yes	$1200 \leq T_s \leq 1600$	only NO
5	No	> 1600	NO and NO ₂
6	Yes	> 1600	NO and NO ₂

145
 146 As input, IU14 needs the natural gas composition C of the fuel input of the flare, the source
 147 temperature T_s (temperature in the combustion zone), and the flare characteristics including
 148 combustion efficiency η (1 is complete combustion without Carbon monoxide formation) and
 149 availability of combustion air δ (above 1 means excess and below 1 means deficiency). In addition
 150 we need the flow rate F , the gauge pressure of the fuel gas in the flare p_g , and the fraction of total
 151 reaction energy that is radiated f . The value for f is estimated by averaging a table of literature
 152 values for f given in Guigard et al. (2000). The IU14 input is summarized in Tab. 2.

153
 154 **Tab.2.** Variables and parameters needed for IU14 or for deriving the fluxes of the air pollutants
 155

Parameter	Description	Reference	Unit
C	Natural gas composition	Sonibare and Akeredolu (2004)	%
T_s	Source temperature	VNF _{flare} (VIIRS, 2015a)	K
η	Combustion efficiency	0.8 (IU14)	-
δ	Availability of combustion air	0.95 (IU14)	-
H	Radiant heat	VNF _{flare} (VIIRS, 2015a)	MW
F	Flow rate	VNF _{flare} (VIIRS, 2015a), (VDI 3782, 1985)	m ³ s ⁻¹
p_g	Gauge pressure	34.475 (API, 2007)	kPa
f	Fraction of radiated heat	0.27 (Guigard et al., 2000)	-

156
 157 The natural gas composition is taken from Sonibare and Akeredolu (2004). They have measured the
 158 molar composition of Nigerian natural gas in the Niger Delta area for ten gas flow stations. For this
 159 study we have calculated the average over these stations and merged the data according their
 160 number of carbon atoms (Tab. 3). H₂S fraction is rather low because it was detected only in two out
 161 of the ten flow stations.

162
 163 **Tab.3.** Molar composition of natural gas in Niger Delta (Nigeria) based on the measurements of Sonibare and Akeredolu
 164 (2004), averaged over ten flow station. The hydrocarbons are merged according to the number of C atoms.
 165

Constituent	Fraction (%)
Methane (CH ₄)	78.47
Ethane (C ₂ H ₆)	6.16
Propane (C ₃ H ₈)	5.50
Butane (C ₄ H ₁₀)	5.19
Pentane (C ₅ H ₁₂)	3.95
Hexane (C ₆ H ₁₄)	0.36
Carbon dioxide (CO ₂)	0.305

Nitrogen (N ₂)	0.06
Hydrogen sulfide (H ₂ S)	0.005

166

167 The source Temperature T_S is taken from VNF_{flare} . The combustion efficiency η and the availability of
 168 combustion air δ significantly depend on the flaring characteristics (e.g. available technique to steer
 169 the flaring process and how the staff takes care of the flaring procedure), which can vary significantly
 170 from one side to another. For SWA no information about these parameters is available. The
 171 parameter range at least was isolated according to literature values for gas flaring in general (not
 172 specifically for SWA). IU14 remarked, that the reaction condition for flaring of $\eta \gg 0.5$ and $\delta \geq 0.9$
 173 should be the norm in regions, where the effective utilization of this gas is not available or not
 174 economically. Strosher (2000) indicates a combustion efficiency of solution gas at oil-field battery
 175 sites between 0.62 and 0.82, and 0.96 for flaring of natural gas in the open atmosphere under
 176 turbulent conditions. EPA (1985) shows combustion efficiencies between 0.982 and 1 for
 177 measurements on a flare screening facility. Based on these information the combustion efficiency η
 178 was set to 0.8. Regarding the availability of combustion air we on the one hand follow IU14 with
 179 $\delta \geq 0.9$ and on the other hand assume that the flaring conditions are not perfect in SWA, which
 180 means that there is a deficiency in combustion air $\delta < 1.0$. Therefore $\delta = 0.9$ was used for this
 181 study. Section 3.3.2 will shed light on the uncertainty which arises from η and δ via a parameter
 182 sensitivity study. The authors strongly recommend a careful selection of η and δ since unrealistic
 183 combinations (e.g. higher combustion efficiencies with rather low availability of combustion air) can
 184 lead to negative NO and NO₂ emissions.

185 The flow rate, gauge pressure and fraction of radiated heat are not included in the parameterization
 186 of IU14 but are necessary to derive the mass emission rates which can be used as emission data for
 187 an atmospheric dispersion model.

188 The flow rate F (m³ s⁻¹) is derived from Eq. 1 (VDI 3782, 1985)

189

$$F = M / (c_p (T_S - T_A)), \quad (1)$$

190

191 where M is the heat flow in MW, c_p the mean specific heat capacity of the emissions, T_S the source
 192 temperature and T_A the ambient temperature. VDI 3782 (1985) provides a value of the mean specific
 193 heat capacity of

194

$$c_p = 1.36 \cdot 10^{-3} \text{ MW s m}^{-3} \text{ K}^{-1} \quad (2)$$

195

196 which is derived for a pit coal firing but VDI 3782 (1985) denotes, that this can be used for other flue
 197 gases as well since potential deviations are negligible. The value is consistent with the derived mean
 198 specific heat capacity for TP15 with an uncertainty below 5%. For the ambient temperature T_A we
 199 use 298.15K as a fixed value, representative for the tropical region. Within a sensitivity study
 200 regarding the influence of T_A on the heat flow, we have used the averaged heat flow and source
 201 temperature of all flares within the time period June/July 2015 and varied the ambient temperature
 202 between 293K and 303K, as a reasonable temperature range in the tropical regions. The resulting
 203 maximum difference in the heat flow is 0.0036 m³ s⁻¹. Therefore we assume that the uncertainties
 204 using a fixed climatological value for the ambient temperature are negligible. For the application of
 205 this inventory to other regions the ambient temperature might be adapted. By using Eq. 1 and 2 the
 206 heat flow F can be derived as

207

$$F = M / (1.36 \cdot 10^{-3} (T_S - 298.15)), \quad (3)$$

208

209 with T_S in K.

210 We assume that the emitted heat flow M is equal to the total reaction energy of the flare. VNF_{flare}
211 only detects the energy fraction that is radiated H and not the total energy M . By using the radiant
212 heat H (observed by VNF_{flare}) and the factor f (fraction of H to the total reaction energy, Guigard et
213 al., 2000), we estimate M as $H \cdot 1/f$. For the source temperature T_S we use the VNF_{flare} observations.
214 The estimation of the fuel gas density, which is necessary to transform the flow rate F into an
215 emission, is problematic due to the lack of data concerning the technical setup of the SWA flares. We
216 assume that the dominating flare type is a low-pressure single point flare. Bader et al. (2011) pointed
217 out that these flares are the most common flare type for onshore facilities that operate at low
218 pressure (below 10 psi (69 kPa) above ambient pressure) and API (2007) remarks that most subsonic-
219 flare seal drums operate in the range from 0 psi to 5 psi (34 kPa). Therefore we have decided for a
220 gauge pressure p_g of 5 psi (34 kPa) above ambient pressure. Via Eq. 3 we can calculate the fuel gas
221 density ρ_f

$$\rho_f = p_f / (R / (M_f T_A)), \quad (3)$$

222
223
224 where p_f is the fuel gas pressure as the sum of ambient pressure (10.1325 kPa, taken as const) and
225 gauge pressure p_g . R is the universal gas constant, M_f the molar mass of the fuel gas and T_A the
226 ambient temperature (298.15 K, taken as const). Finally, the emission E (kg s^{-1}) of a species i is given
227 by
228

$$E_i = \frac{m_i}{m_{total}} \rho_f F, \quad (4)$$

229
230 where m_i is the mass of the species i and m_{total} the total mass of the fuel gas, both delivered by the
231 parameterization of IU14.
232

233 The combustion calculations within IU14 provide the species water, hydrogen, oxygen, nitrogen,
234 carbon monoxide, carbon dioxide, sulfur dioxide, nitrogen oxide and nitrogen dioxide. In the
235 following only the latter five are considered. However, no black carbon or volatile organic
236 compounds (VOCs) are considered by IU14, although they are not negligible. Johnson et al. (2011)
237 estimated the mean black carbon emission for a large-scale flare at a gas plant in Uzbekistan to be
238 7400 g h^{-1} and Strosher (1996) measured the concentration of predominant VOCs 5 m above the gas
239 flare in Alberta with 458.6 mg m^{-3} . However, owing to the missing representation of black carbon and
240 VOCs in IU14, these compounds are not considered in this study.

241 By using the source code written in R (R Core Team, 2013) delivered by this study, the user can define
242 the grid size independently (e.g. model grid) on which the flaring point sources are allocated.

243

244 3. Results

245

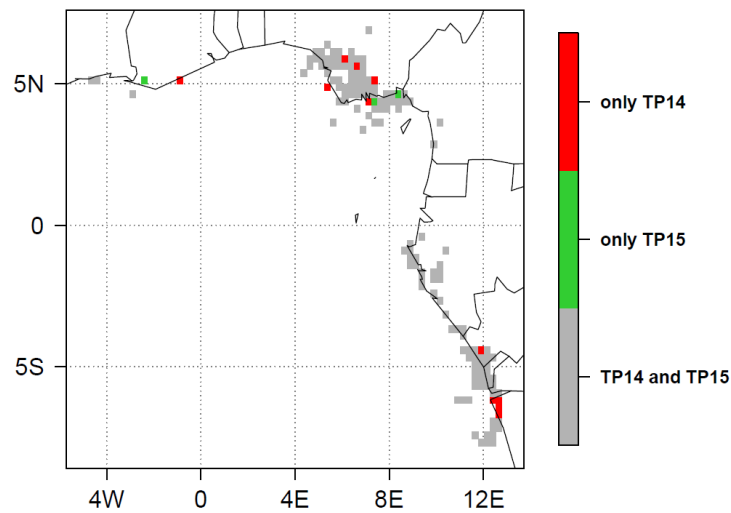
246 3.1 Spatial distribution of gas flaring in SWA

247

248 We have selected the two time periods June/July 2014 (TP14) and June/July 2015 (TP15) of VNF_{flare}
249 over SWA (61 observations respectively).

250 In the preparation of this work we have compared the locations of the flares of TP14 with the Google
251 Earth imagery (Google Earth, 2014) (not shown). Only the onshore flares are visible in Google Earth.
252 This visual verification reveals that 72% of the VNF_{flare} detected onshore flares are visible in Google
253 Earth. It is very likely that the hit rate is much higher since it is often the case that the Google Earth

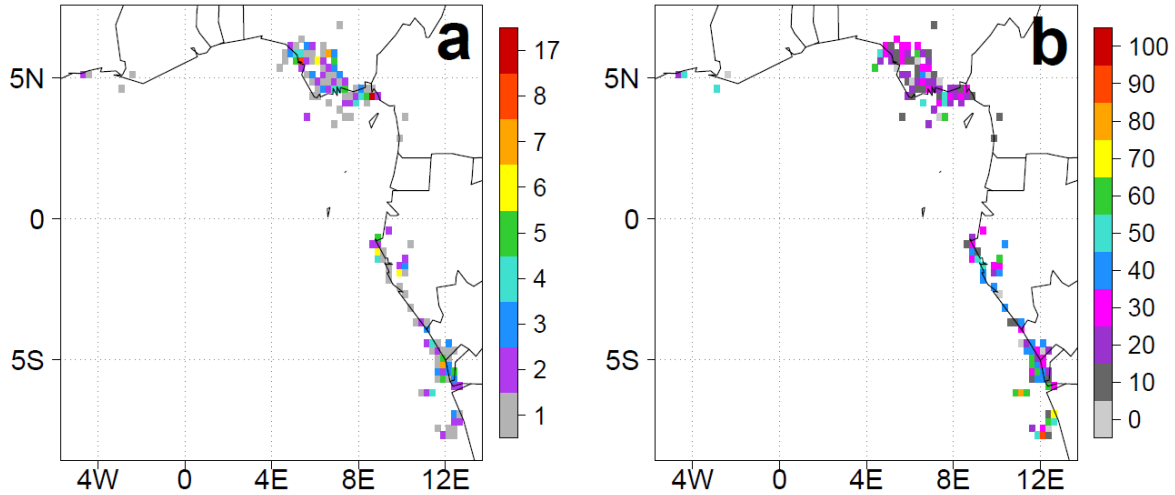
254 image quality is not good enough for verification or the images are not up to date. This comparison
 255 indicates that VNF_{flare} is an effective method to identify the flares in SWA.
 256 For the following analysis we have allocated the flares to a grid with a mesh size of 0.25° (28 km)
 257 from $8^\circ S$ to $7^\circ N$ and from $5^\circ W$ to $13^\circ E$ and calculated the emissions for both time periods. A grid box
 258 with flaring is denoted as flare box hereafter. Fig. 1 emphasizes the areas in which VNF_{flare} detects
 259 flares only in TP14 (TP15) in red (green) color and in grey the areas with flaring in both periods.
 260
 261



262
 263 **Fig.1.** Flaring area for TP14 and TP15. Red (green) boxes denote areas with flaring only for TP14 (TP15). For the grey areas,
 264 flaring is detected in both time periods.
 265
 266

267 Remarkable are the dominating flaring areas in the Niger Delta and the adjacent offshore regions in
 268 the Gulf of Guinea. Also in the coastal region of Gabon, Congo, Angola and sporadically in Ghana and
 269 offshore of Ivory Coast, flaring occurs. By comparing TP14 and TP15 more red than green areas are
 270 visible, especially in southern Nigeria, which indicates a reduction in the flaring area from 2014 to
 271 2015. The red areas contribute 12% to the total CO_2 emissions of TP14. VNF_{flare} detects 335 flares in
 272 2014 and 312 flares in 2015 which means a reduction of about 7% (counted are those which deliver
 273 at least once a value for T_s and H in the time period). 61% of that reduction is related to Nigeria. A
 274 decrease in CO_2 from 1994 to 2010, particularly in the onshore platforms is indicated by Doumbia et
 275 al. (2014).

276 Fig. 2 shows the density of flares (a) and the flaring activity (b) per flare box for TP15. The results are
 277 similar to TP14, therefore only the TP15 is displayed here.
 278



279
280
281
282
283

Fig.2. (a) Number of flares per flare box and (b) flaring activity (%) per flare box within TP15. A flaring activity of 100% means that every day on the 61 day period in June/July flaring was detected.

284 The highest flare density can be found offshore in the border area of Nigeria and Cameroon with 17
285 flares per flare box. The offshore flaring density is smaller than onshore (Fig. 2a) whereas the highest
286 flaring activity can be found offshore (Fig. 2b). This could be linked to the increased masking of flares
287 by clouds over land. The large onshore flaring area of the Niger Delta shows a comparable low flaring
288 activity of 10-30%. Highest values can be found offshore of the Democratic Republic of the Congo
289 and Angola of 50-90%. How the interannual variability of flaring reflects in the amount of flaring
290 emissions is analyzed in section 3.3.4.

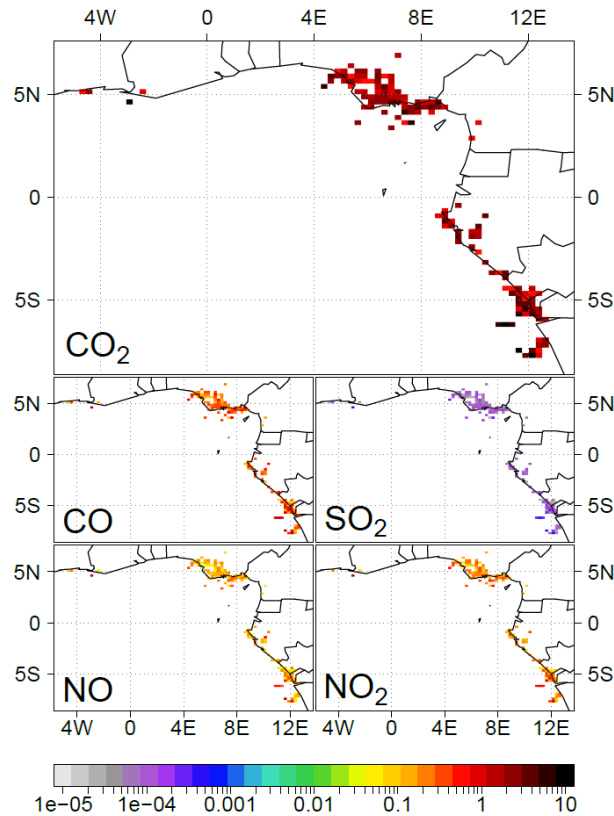
291

3.2 Emission estimation

292
293

294 For the emission estimation we have used a climatological approach (E_{clim}). For every flare the
295 temporal averages of source temperature and radiant heat over TP14 and TP15 were used to
296 calculate the emissions. Therefore in this approach all flares, detected in the time period, are active
297 at once with their mean emission strength. This method has the advantage that most likely all flares
298 in the domain are captured even if a fraction of them is covered by clouds at certain days. However,
299 this could lead to an emission overestimation because not all available flares are active at once. This
300 problem of separating between flares which are not active and flares which are active but covered by
301 clouds and therefore not visible for VNF_{flare} is picked up again in Section 3.3.1. Fig. 3 shows the
302 emissions of CO_2 , CO , SO_2 , NO and NO_2 in t h^{-1} for TP15.

303



304
305
306
307
308

Fig.3. Flaring emissions for TP15 within E_{clim} in t h^{-1} considering CO_2 , CO, SO_2 , NO and NO_2 . For better visibility the emissions are displayed as colored grid boxes although the emissions are still point sources and not area sources.

309 Highest emissions are derived for carbon dioxide, followed by carbon monoxide, nitrogen dioxide
310 and nitrogen oxide. Sulfur dioxide shows lowest emissions since these emissions do not depend on
311 combustion processes but only on the natural gas composition (see Tab. 3) and the amount of flared
312 gas (IU14). Due to the use of the averaged measurements of Sonibare and Akeredolu (2004), local
313 variations of hydrogen sulfide concentrations in the natural gas cannot be taken into account.
314 Hydrogen sulfide is the only source of sulfur in the flared gas and therefore determines the emission
315 of sulfur dioxide. To assess this uncertainty, a sensitivity study with different hydrogen sulfide
316 concentrations is given in Section 3.3.5.

317

318 3.3 Estimation of uncertainties

319

320 In the following section the most relevant uncertainties are presented together with approaches for
321 their assessment. This includes the uncertainty concerning the flare detection in the presence of
322 cloud cover, the uncertainty in the determination of the emitted heat flow H via the fraction of
323 radiated heat f , the uncertainty in the choice of the IU14 parameters and the changes in flare
324 operation from one year to another as well as the influence of the spatial variability of hydrogen
325 sulfide in the natural gas on the sulfur dioxide emissions. Apart from Section 3.3.4 all uncertainty
326 estimations are confined to TP15.

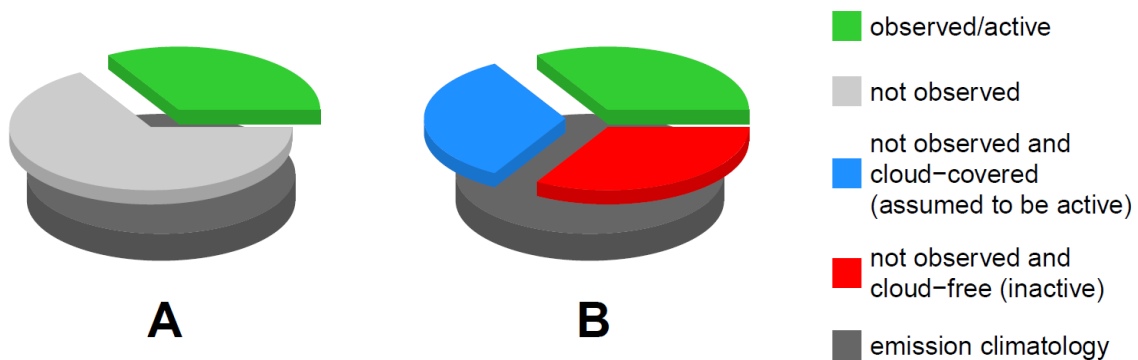
327

328 3.3.1 Uncertainty due to cloud cover

329

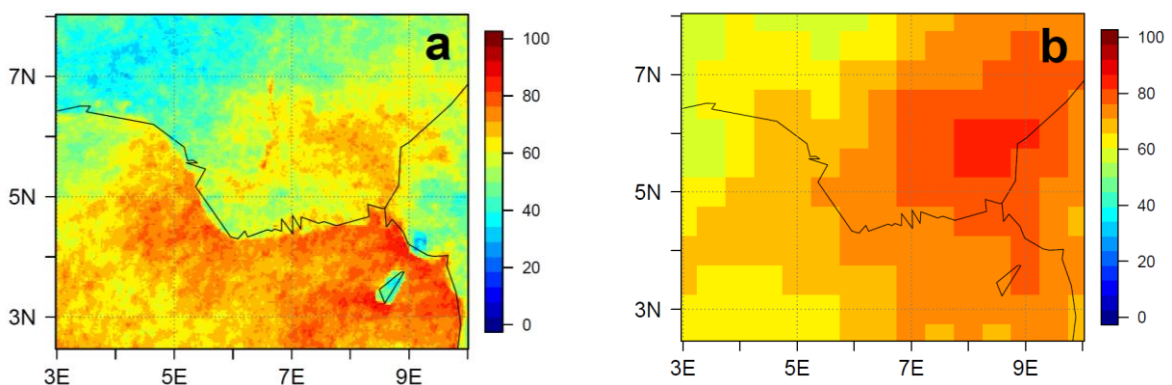
330 In this section we want to estimate the emission error due to cloud-covered flares and present a
331 method to derive daily emissions by considering the contribution of these masked flares. In Section

332 3.2 a climatological data set of flaring emissions (E_{clim}) was derived, in which all available flares are
 333 active with their mean emission strength. This dataset therefore does not include a day to day
 334 variation. If an emission dataset with a daily variability is required, the problem arises that usually
 335 parts of the scene observed by the satellite are covered by clouds and therefore the emissions are
 336 likely underestimated. VNF_{flare} includes the locations of all flares independent whether there are
 337 active or not. This entity is illustrated by the closed dark grey pie in Fig. 4A and 4B. By comparing the
 338 flares which are observed/active at a certain day and the total number of flares, a separation
 339 between observed (green pie in Fig. 4A) and not observed (light grey pie in Fig. 4A) is possible. In
 340 addition VNF_{flare} delivers a cloud mask for all of the flare detections. Therefore it is possible to
 341 separate the light grey pie of the not observed flares in (a) cloud-free and inactive (light blue pie in
 342 Fig. 4B) and (b) cloud-covered and unknown flaring status (blue pie in Fig. 4B).
 343 To estimate the error due to active but cloud-covered flares, we assume that all of these flares are
 344 active with their mean emission strength observed in June/July 2015.
 345



346
 347 **Fig.4.** Pie charts illustrating the flaring emission uncertainty assessment due to cloud cover for TP15. The entity of the flares
 348 within the emission climatology (E_{clim}) is given as closed grey pie in the bottom of **A** and **B**. **A** distinguishes between flares
 349 which are detected/active at a certain day (green) and the complement of undetected flares (light grey). In **B** the light grey
 350 slice of **A** is separated in a cloud-covered (blue) and cloud-free (red) part by using the cloud mask of VNF_{flare} . Flares which
 351 are not detected by VNF_{flare} and covered by clouds are taken as active. Flares which are not detected by VNF_{flare} and are not
 352 covered by clouds are taken as inactive.
 353
 354

355 Fig. 5 illustrates the mean cloud cover exemplarily for the greater Niger Delta area using (a)
 356 instantaneous cloud fractional cover (CFC) from the geostationary Meteosat Second Generation 3
 357 (MSG3) (CM SAF, 2015, copyright (2015) EUMETSAT) for every day of TP15 around the time of VNF
 358 observation (Suomi-NPP overflight approx. at 1 UTC) and (b) the sun-synchronous Aqua/AIRS
 359 (Mirador, 2016).
 360



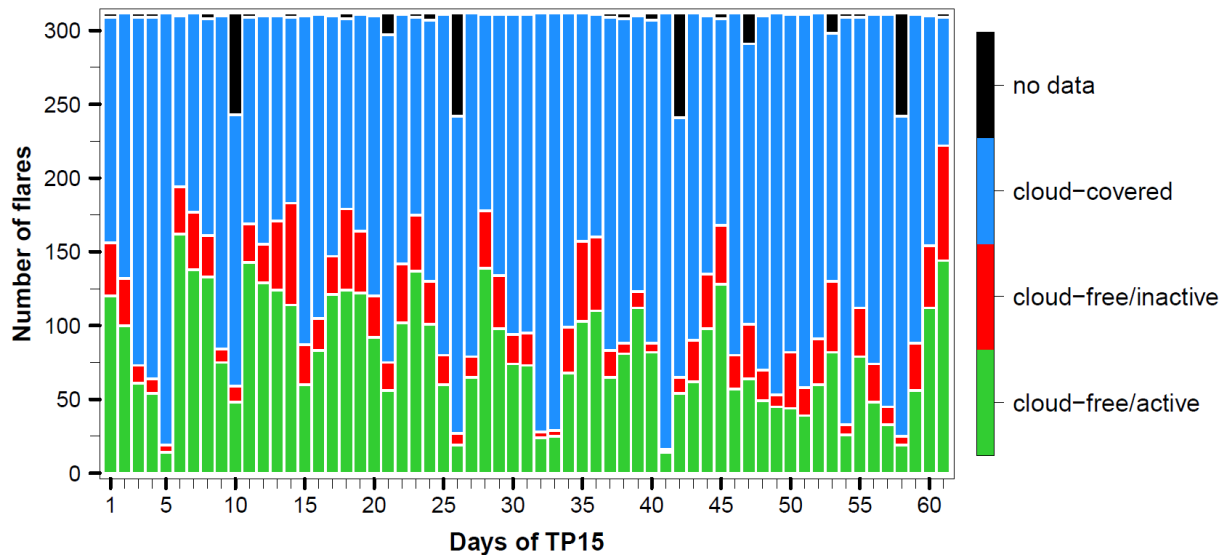
362 **Fig.5.** Fractional cloud cover (%) observed from (a) the geostationary MSG3 and (b) the sun-synchronous Aqua/AIRS,
 363 averaged over TP15 around the time of VNF observation (approx. 1 UTC).

364

365 Fig. 5a shows that the onshore flaring area for TP15 is in mean covered with clouds by 50-70%. For
 366 the offshore flaring area it is even higher with 70-90%. Therefore it is very likely that flares are
 367 frequently masked by clouds and therefore not detected by VNF. However, we suspect that the
 368 MSG3 cloud product underestimates (overestimates) the onshore (offshore) cloud cover when
 369 comparing with the findings of van der Linden et al. (2015). The high offshore coverage and the
 370 distinct land-water separation might be caused by overestimating low clouds in the presence of a
 371 warm and moist tropical ocean.

372 Fig. 5b shows a cloud climatology using Aqua/AIRS Nighttime data (Mirador, 2016). The Aqua/AIRS
 373 climatology shows higher cloud cover over land and no distinct separation between water and land
 374 surface. Both products identify the highest onshore cloud cover in the northeast of Port Harcourt
 375 (4.8°N, 7.0°E) and have similar values in the Nigerian offshore region (containing the offshore flares)
 376 of about 70-80%. The major difference in the climatologies appears onshore between 4.5°N and 6°N.
 377 This area includes the majority of the Nigerian onshore flares. This reveals a relatively high
 378 uncertainty in the estimation of nocturnal low cloud coverage from remote sensing.

379 Fig. 6 shows the number of flares per day in TP15, separated in the categories: cloud-free/active
 380 (green), cloud-free/inactive (red) and cloud-covered (blue). Flares with no or incomplete data are
 381 coded in black. E_{clim} includes 312 flares which are at least once active in TP15. On average only 26% of
 382 the total flaring area is active at once, 9% is verifiable inactive and 63% is cloud-covered. By taking
 383 into account only the cloud-free information instead of the climatological approach of E_{clim} , on
 384 average 63% of the flares are not considered at a certain day. By assuming that all of these cloud-
 385 covered flares are active, a remarkable underestimation can be expected.



386

387 **Fig.6.** Number of flares per day in TP15 which are cloud-free and active (green), cloud-free and inactive (red) and cloud-
 388 covered (blue). Flares with no or incomplete data are denoted in black. The color coding follows Fig. 4B. Considered are the
 389 312 flares which deliver at least once a value for T_s and H in TP15.

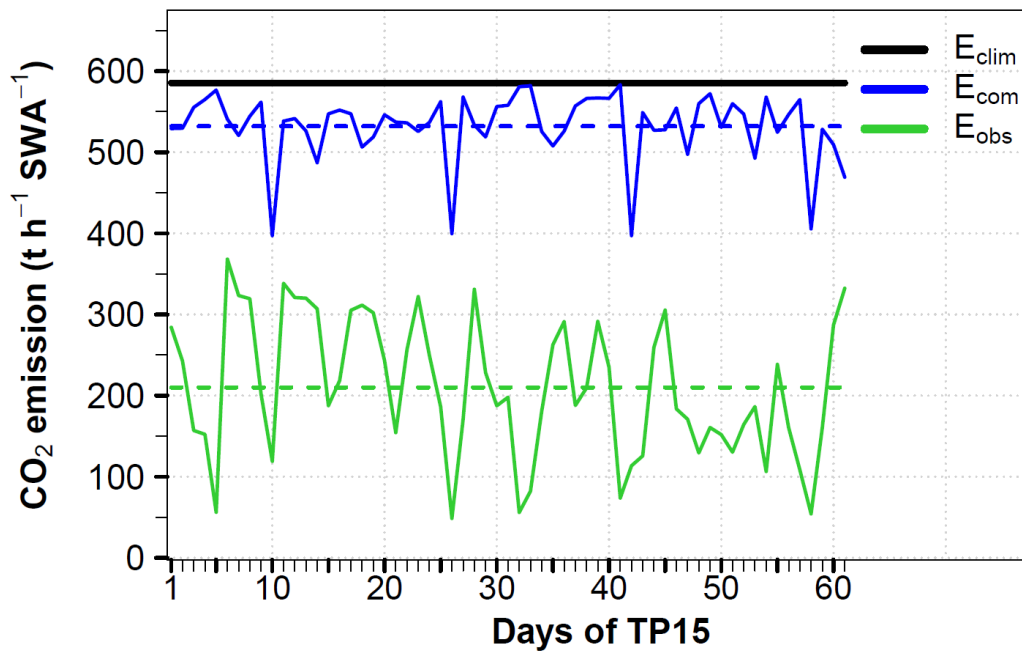
390

391 In addition to E_{clim} two further emission inventories are introduced: E_{obs} only considers the actual
 392 daily observed flares (linked to the green flares in Fig. 6). To consider also the contribution of active
 393 but cloud-covered flares, E_{com} combines the green and the blue flares of Fig. 6.

394 To allow for consistency, all three inventories use the emissions derived from the flare specific
 395 temporal averages of the source temperature and the radiant heat over TP14 and TP15 respectively.

396

397 We avoid calculating the emissions from instantaneous source temperatures because this is linked to
 398 high uncertainty depending on the atmospheric conditions (Mikhail Zhizhin, personal
 399 communication). The temporal averages allow for robustness. Therefore the three inventories only
 400 differ in the selection of the active flares per day but not in the underlying emissions. E_{clim} uses all
 401 flares at a certain day, E_{obs} considers only the flares which are cloud-free and active and E_{com}
 402 considers E_{obs} plus the cloud-covered flares, by assuming that all of the cloud-covered flares are
 403 active. Nevertheless we have included a further inventory in Tab. 5 which uses instantaneous source
 404 temperature and radiant for the emission derivation (E_{clim} , instant. input) to assess the differences
 405 towards the averaged input. Fig. 7 shows the total CO₂ emissions of the SWA area from E_{clim} in black,
 406 from E_{obs} in green and from E_{com} in blue.
 407



408
 409 **Fig.7.** Daily CO₂ emission estimations (t h⁻¹) within TP15 from flaring, summed up over the SWA area as denoted in Fig. 1 for
 410 the three emission inventories: E_{clim} (climatology, black solid line), E_{obs} (daily VNF_{flare} observations, green solid line and
 411 temporal average as green dashed line) and E_{com} (sum of daily VNF_{flare} observations and emissions from cloud-covered
 412 flares, blue solid line and temporal average as blue dashed line). The periodical drop of the blue line is linked to reduced
 413 data coverage (compare with black bars in Fig. 6).
 414
 415

416 The dashed lines denote the temporal averages of E_{obs} and E_{com} . On average E_{com} is only 9% smaller
 417 than E_{clim} which is assumed to be in the range of uncertainty. Therefore both inventories are
 418 equitable in this study. The user can decide whether a temporal resolved or a climatological
 419 approach fits best to their research question.

420 The emissions of E_{obs} are strongly reduced (64%) compared to E_{clim} as expected. The use of E_{obs} would
 421 significantly underestimate the emissions and is therefore not appropriate for an application. Since
 422 E_{obs} does not take into account cloud-covered flares at all and E_{com} in contrast sees all cloud-covered
 423 flares as active, the difference between these inventories can be used to assess the uncertainty
 424 arising from flares masked by clouds. Fig. 7 shows a mean difference between E_{obs} and E_{com} of about
 425 61%. Therefore while using E_{obs} as a flaring emission inventory in an application, an underestimation
 426 of the emissions of 61% has to be considered.

427 These emission estimations contain different information. E_{clim} includes all flares of the domain
 428 invariant but can overestimate the emissions. E_{obs} shows the VNF_{flare} reality, including a temporal

429 development, but cannot consider the cloud-covered flares. E_{com} combines the climatological
 430 information of E_{clim} for flares which are not observable at a certain time and the temporal resolution
 431 of VNF_{flare} in E_{obs} . However this approach is based on the assumption that all cloud-covered flares are
 432 active, which can be seen as an estimation upwards. Therefore the most likely amount of emissions is
 433 expected between E_{obs} and E_{com} .

434

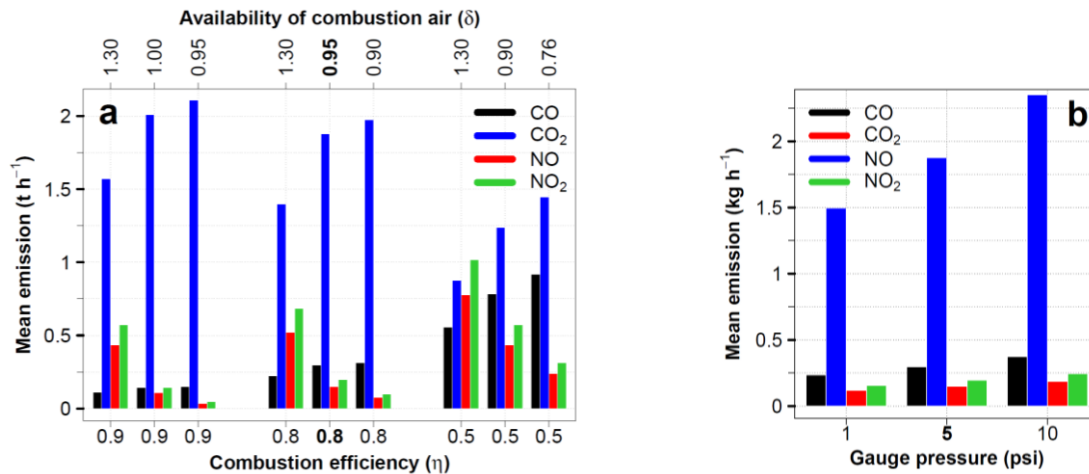
435 3.3.2 Uncertainty due to IU14 input parameters

436

437 To assess the uncertainty which arises from the combustion efficiency η and the availability of
 438 combustion air δ , a sensitivity study has been carried out. The exact values for the SWA flares are
 439 unknown and very likely highly variable from one flare to another, depending on the flare type and
 440 operation. Fig. 8a shows the flaring emissions averaged over SWA and TP15 for CO, CO₂, NO and NO₂.
 441 The parameters η and δ are varied referring to IU14. A complete combustion ($\eta = 1$) does not
 442 produce CO emissions since all carbon is transformed to CO₂ (not shown). With decreasing η and δ ,
 443 the CO and CO₂ emissions increase. Concerning CO we assume the lower limit for $\eta = 0.9$ and
 444 $\delta = 1.3$ (left of Fig. 8a) and the upper limit for $\eta = 0.5$ and $\delta = 0.76$ (right of Fig. 8a). The values
 445 used for this study are located in the center of Fig. 8a (printed in bold). By taking the latter as
 446 reference, the lower (upper) limit leads to a decrease (increase) in CO emission of -63% (+208%). For
 447 CO₂ we derived an lower (upper) limit of -53% (+12%).

448 A higher availability of combustion air allows an enhanced formation of NO and NO₂. Therefore NO_x
 449 emissions increase with decreasing η . In contrast these emissions decrease with an increase in the
 450 combustion efficiency (δ). The higher the efficiency the more oxygen is forming CO₂ instead of NO_x.
 451 We assume the lower limit for $\eta = 0.9$ and $\delta = 0.95$ and the upper limit for $\eta = 0.5$ and $\delta = 1.30$.
 452 Taking again the central parameter set of Fig. 8a as reference, the lower (upper) limit leads to a
 453 decrease (increase) in NO emission of -76% (+420%).

454



455

456 **Fig.8.** Flaring emissions ($t h^{-1}$) spatiotemporally averaged over SWA and TP15 depending on (a) combustion efficiency η and
 457 availability of combustion air δ for a gauge pressure of 5 psi and (b) gauge pressure (psi) for $\eta = 0.8$ and $\delta = 0.95$. SO₂ is
 458 not shown because it does not depend on η or δ .

459

460 For NO₂ the emission decrease (increase) is -76% (+417%).

461 In addition, Fig. 8b shows the emissions depending on the gauge pressure for 1 (lower limit), 5 and
 462 10 psi (upper limit) (7, 34 and 69 kPa respectively) for $\eta = 0.8$ and $\delta = 0.95$. Using 5 psi as the
 463 reference, the lower (upper) limit leads to a decrease (increase) in CO emissions of -20% (+25%).

464 Fig. 8 emphasizes that the technical conditions of flaring crucially influence the emission strength and
 465 that the emissions are more sensitive towards η and δ than towards the gauge pressure.

466

467 3.3.3 Uncertainty due to the fraction of radiated heat

468

469 To estimate the uncertainty in the fraction of radiated heat f (see Tab. 2), we have used the standard
 470 deviation of the literature values given in the appendix of Guigard et al. (2000) in addition to the
 471 mean value of $f = 0.27$. This leads to a domain of uncertainty for the value f of $(^{0.38}/_{0.16})$. Therefore
 472 the VNF_{flare} observed radiant heat is multiplied with the factor $1/f$ of 3.7 ($^{6.2}/_{2.6}$).

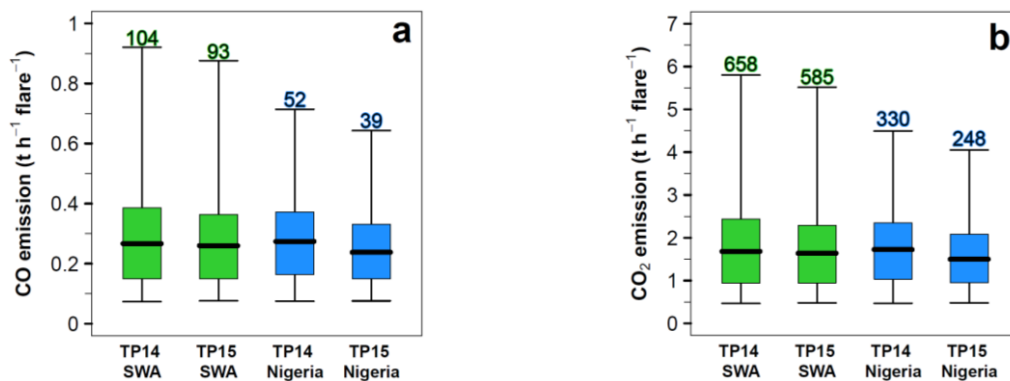
473

474 3.3.4 Interannual variability

475

476 The differences in flaring between TP14 and TP15, indicated in Fig. 1 and Fig. 2, are quantified in this
 477 section according to the emissions of CO (Fig. 9a) and CO₂ (Fig. 9b). The boxplots include all flares for
 478 the two domains SWA (green) and Nigeria (blue). The numbers above indicate the integrated
 479 emissions per hour and area in tons.

480



481 **Fig.9.** Single flaring emissions of (a) CO and (b) CO₂ (E_{clim} , $\text{t h}^{-1} \text{ flare}^{-1}$) for SWA (green) and Nigeria (blue) for TP14 and TP15.
 482 The values above the boxplots indicate the emissions per hour, integrated over SWA (green) and Nigeria (blue). The
 483 whiskers span the data range from the 0.025-quantile to the 0.975-quantile (95% of the data). Data outside of this range is
 484 not shown.

485

486
 487 The emissions of CO₂ are 6.3 times higher than the CO emissions. For Nigeria (blue boxplots) the
 488 mean value of emissions is statistically significant lower for TP15 compared to TP14 (Wilcoxon-Mann-
 489 Whitney rank sum test with a significance level of 0.05). For SWA the emission averages show no
 490 significant difference. The significant different mean values for Nigeria emphasize the relevance of
 491 using a flaring dataset which is up to date to reduce uncertainties arising from deviations in flare
 492 locations or flaring processes.

493

494 3.3.5 Uncertainty due to spatial variability in H₂S

495

496 Since hydrogen sulfide (H₂S) is the only sulfur source in the flared gas, it determines the emission of
 497 sulfur dioxide. The natural gas composition measurements from the ten flow stations given in
 498 Sonibare and Akeredolu (2004) contain only two stations with nonzero H₂S content. Therefore
 499 averaging over the ten stations (see Tab. 3) leads to a low H₂S content in the emission calculations.
 500 By using the highest concentration value of H₂S given in Sonibare and Akeredolu (2004) (see Tab. 3,
 501 H₂S concentration 0.03% instead of 0.005%), we try to estimate the upper limit of SO₂ emission,
 502 assuming that all flares are provided with this more sulfur containing gas. With this approach the

503 temporal averaged sum of SO₂ emissions over SWA increase from 36 to 320 kg h⁻¹. This comparison
 504 reveals that among the flaring conditions also the natural gas composition plays an important role in
 505 estimating the flaring emissions reasonably. To rely on a single measurement dataset for a large
 506 flaring domain and without taking into account spatial variability is therefore problematic but has to
 507 be accepted owing to data shortage.

508 This section has estimated the uncertainties in gas flaring due to cloud cover, parameters of IU14, the
 509 fraction of radiated heat, the temporal variability and the H₂S concentration in the natural gas. The
 510 uncertainty regarding the spatial variability of the total hydrocarbon fraction of the natural gas,
 511 which is estimated by the variations in the ten flow station measurements of Sonibare and Akeredolu
 512 (2004), is below 1%.

513 However, there are further assumptions or sources of uncertainty which cannot be quantified within
 514 this study: We assume that the natural gas composition, which is measured in one region, is valid for
 515 SWA entirely. The gas flares are taken as constant emission sources because VNF_{flare} only provides
 516 one observation (overflight) per day. We cannot take into account the spatial variability of the flares
 517 concerning the IU14 parameters and the stack heights. And finally IU14 delivers no VOCs and black
 518 carbon.

519

520 4. Comparison with existing emission inventories

521

522 The following section places the estimated flaring emissions of this study in the context of existing
 523 emission inventories, by taking the focus on CO₂. A direct comparison with existing emission
 524 inventories is problematic due to different reference time periods, spatial domains, definitions of
 525 emission sectors and the limitation of chemical compounds. Tab. 5 summarizes the CO₂ emissions for
 526 different inventories regarding Nigeria as the flaring hotspot of the research domain. To derive
 527 annual emission values for the results of this study, it is assumed that the flaring emission conditions
 528 of TP14 and TP15 are representative for the whole year 2014 and 2015 respectively. Therefore the
 529 hourly emissions are integrated over 365 days. In addition to the three inventories E_{obs}, E_{com} and E_{clim},
 530 whose emissions are derived from temporal averages of the source temperature and radiant heat,
 531 also an emission estimation using instantaneous source temperature and radiant heat (calculating
 532 emissions for every single observation and subsequent temporal averaging of the emissions) for both
 533 time periods is presented in Tab.5 (E_{clim}, instant. input).

534

535 **Tab.5.** Comparison between existing emission inventories for CO₂ (with a focus on gas flaring if available) and the results of
 536 this study for Nigeria in teragram (Tg) per year. For TP14 and TP15 it is assumed that the two month observations represent
 537 the flaring conditions of the whole year 2014 and 2015 respectively. Therefore the emissions were integrated to yearly
 538 values. The domain of uncertainty arising from the UP14 parameters and the spatial variability in total hydrocarbon is given
 539 in brackets. For the fraction of radiated heat *f*, the mean value 0.27 and the lower (upper) boundary of 0.16 (0.38) are
 540 used, representing a further source of uncertainty. The products given in bold are directly related to flaring emissions.

541

Emission inventory	Time period	CO ₂ emissions (Tg y ⁻¹)		
		<i>f</i> = 0.16	<i>f</i> = 0.27	<i>f</i> = 0.38
This study (E_{obs}, averaged)	2014 (from TP14)	1.7 (2.2/0.3)	1.0 (1.3/0.2)	0.7 (1.0/0.1)
This study (E_{com}, averaged)	2014 (from TP14)	4.5 (6.1/0.9)	2.7 (3.6/0.5)	1.9 (2.6/0.3)
This study (E_{clim})	2014 (from TP14)	4.9 (6.5/1.0)	2.9 (3.9/0.6)	2.1 (2.8/0.4)
This study (E_{obs}, averaged)	2015 (from TP15)	1.0 (1.4/0.2)	0.6 (0.8/0.1)	0.4 (0.6/0.0)
This study (E_{com}, averaged)	2015 (from TP15)	3.4 (4.5/0.7)	2.0 (2.7/0.4)	1.4 (2.0/0.3)
This study (E_{clim})	2015 (from TP15)	3.7 (4.9/0.7)	2.2 (2.9/0.4)	1.5 (2.1/0.3)
This study (E_{clim}, instant. input)	2014 (from TP14)	9.9 (13.2/2.0)	5.9 (7.9/1.2)	4.2 (5.6/0.8)

This study (E_{clim}, instant. input)	2015 (from TP15)	8.8 (^{11.8} / _{1.8})	5.2 (^{7.0} / _{1.0})	3.7 (^{4.9} / _{0.7})
CDIAC (2015b)¹	2011		27.47	
EIA (2015)²	2010; 2011; 2013		38.81; 41.39; 52.83	
Doumbia et al. (2014)¹	2010		45	
EDGAR 4.2³ (ECCAD, 2015)	2008		8.75	
EDGAR 4.2⁴ (ECCAD, 2015)	2008		3.50	
EDGAR 4.3.2⁵ (EDGAR, 2016)	2010; 2011; 2012		29.4, 28.8, 28.9	
EDGARv43FT2012⁶ (EDGAR, 2014)	2014		93.87	

¹from gas flaring, Nigeria

²from consumption and flaring of natural gas

³from refineries and transformation, Nigeria

⁴from refineries and transformation, Niger Delta area according to Fig. 5a

⁵from venting and flaring of oil and gas production, Nigeria

⁶emission totals of fossil fuel use and industrial processes (cement production, carbonate use of limestone and dolomite, non-energy use of fuels and other combustion). Excluded are: short-cycle biomass burning (such as agricultural waste burning) and large-scale biomass burning (such as forest fires), Nigeria

542
543
544
545
546
547
548
549
550
551

The CO₂ emission estimations of this study are given in Tab. 5 together with an overall uncertainty range of (⁺³³/₋₇₉%) in brackets, including the uncertainty from the IU14 parameters η and δ (⁺¹²/₋₅₃%) and the gauge pressure (⁺²⁰/₋₂₅%) and from spatial variability of total hydrocarbon. The latter uncertainty is small (below 1%) owing to the low variation in THC concentration in the measurements of Sonibare and Akeredolu (2004). The uncertainty owing to the fraction of radiated heat f is represented by using the average value of 0.27 and the upper and lower estimate of 0.16 and 0.38 respectively. The uncertainty due to cloud cover is represented by the difference in E_{obs} and E_{com} .

552
553
554
555
556
557
558
559
560
561
562
563
564
565
566
567
568
569
570

By assuming that E_{com} with $f = 0.27$ represents the best emission estimate for this study and by integrating the above mentioned sources of uncertainty, a total Nigerian CO₂ flaring emission of 2.7 (^{3.6}/_{0.5}) Tg y⁻¹ for 2014 and 2.0 (^{2.7}/_{0.4}) Tg y⁻¹ for 2015 was derived. Due to the high uncertainties, the two estimates are not statistically different. These values are one order of magnitude smaller than the values from the Carbon Dioxide Information Analysis Center (CDIAC, 2015b), the Energy Information Administration (EIA, 2015) and the EDGARv.4.3.2 (EDGAR, 2016) database. A direct comparison is hindered by a time lag of 3-4 years and missing information about the uncertainties of CDIAC. The values of EIA are higher than those of CDIAC because EIA includes the consumption of natural gas in addition to gas flaring. Doumbia et al. (2014) combines Defense Meteorological Satellite Program (DMSP) observations of flaring with the emission factor method to derive flaring emissions. The results agree with EIA (2015) but are 64% higher than CDIAC (2015b).

571
572
573

The emission inventory EDGAR v4.2 (ECCAD, 2015) delivers 8.75 (3.50) Tg CO₂ y⁻¹ for Nigeria (Niger Delta area) for the emission sector *refineries and transformation*, which is in good agreement with the results for the study on hand.

574
575
576
577
578
579

As a benchmark for the flaring CO₂, the total CO₂ emissions for Nigeria are given by EDGAR (2014), (fossil fuel use and industrial processes). Taking EDGAR (2014) as a reference for total CO₂ emissions of Nigeria, flaring emissions contribute with 2 (^{3.9}/_{0.0})% (this study for 2014; E_{com}), 9% (2008; ECCAD, 2015), 28% (2011; CDIAC, 2015b), 48% (2010; Doumbia et al., 2014) or 56% (2013; EIA, 2015). The large spread between the different inventories emphasizes the large uncertainty within the estimation of emissions from gas flaring.

580
581
582

By using the climatological approach with instantaneous source temperature and radiant heat input data (E_{clim} , instant. input) instead of temporal averages (E_{clim}), the emissions are increased by approx. a factor of two (5.9 (^{7.9}/_{1.2}) Tg y⁻¹ for 2014, 5.2 (^{7.0}/_{1.0}) Tg y⁻¹ for 2015). This underlines that also the

583 preprocessing of the remote sensing data for the calculation of the emissions is a considerable
584 source of uncertainty. However, due to the high uncertainties also the two emission estimates with
585 and without instantaneous data are not statistically different.

586 A shortcoming of the PEGASOS_PBL-v2 (not shown) and the EDGAR v4.2 emission inventory is the
587 lack of offshore flaring emissions in the Gulf of Guinea south of Nigeria. For CDIAC and EIA this
588 cannot be verified since the data is only available as a single value per country.

589 The differences between the results of this study and the existing emission inventories might be
590 caused by insufficient information about the efficiency of combustion processes of SWA flares or by
591 an inconsistent definition of emission source sectors for the existing inventories. E_{com} , Doumbia et al.
592 (2014) and CDIAC (2015b) focus on gas flaring, whereas other products also include natural gas
593 consumption and emissions from refineries and transformation, which also can include non-flaring
594 emissions within and outside the areas indicated as flaring area by the satellite imagery. In addition,
595 the existing inventories do not provide current values (time lag of 2 to 6 years) and therefore not
596 consider the emission reduction indicated by Fig. 9.

597

598 **5. Discussion and conclusions**

599

600 The gas flaring emission estimating method of Ismail and Umukoro (2014) (IU14) has been combined
601 with the remote sensing flare location determination of the VIIRS Nightfire Prerun V2.1 Flares only
602 (VNF) (VIIRS, 2015a) for a new flaring emission parameterization. The parameterization combines
603 equations of incomplete combustion with the gas flow rate derived from remote sensing parameters
604 instead of using emission factors and delivers emissions of the chemical compounds CO, CO₂, SO₂, NO
605 and NO₂.

606 Within this study the parameterization was applied to southern West Africa (SWA) including Nigeria
607 as the second biggest flaring country. Two two-month flaring observation datasets for June/July 2014
608 (TP14) and June/July 2015 (TP15) were used to create a flaring climatology for both time periods. In
609 this climatology all detected flares emit with their mean activity (climatological approach).

610 The uncertainties owing to missed flare observations by cloud cover, parameterization parameters,
611 interannual variability and the natural gas compositions were assessed. It can be shown that the
612 highest uncertainties arise from the IU14 parameters ($+^{33}/_{-79}$ %), followed by the definition of the
613 fraction of radiated heat f . The uncertainty arising from flares masked by clouds is estimated as 61%
614 on average in TP15.

615 By using the cloud detection of VNF and by assuming that all cloud-covered flares are active, an
616 additional emission dataset was derived which combines the emissions from the currently observed
617 flares and the climatological emissions from cloud-covered (not detected) flares (combined
618 approach). These emissions are on average 9% smaller than the climatology but 61% larger than the
619 net observations.

620 However, owing to the large uncertainty ranges, no significant difference between the climatological
621 inventory and the combined inventory can be stated. Comparing the emissions of 2014 and 2015, a
622 reduction in the flaring area, density of active flares and a significant reduction in Nigerian flaring
623 emissions about 25% can be observed, which underlines the need for more recent emission
624 inventories.

625 The uncertainty due to the natural gas composition is compound dependent. The spatial variation in
626 total hydrocarbon is negligible but the availability of hydrogen sulfide, which exclusively determines
627 the amount of emitted SO₂, cause large uncertainty. By taking the combustion efficiency to derive
628 the fraction of unburned natural gas, the amount of emitted VOCs might be estimated in addition to

629 the species of the study on hand but would also be linked to high uncertainties concerning the VOC
630 speciation. The uncertainty in VOC emission is increased drastically by natural gas which is vented
631 directly into the atmosphere instead of being flared, since the venting cannot be detected by VNF.
632 With a focus on Nigeria, the CO₂ emission estimates of this study were compared with existing
633 inventories. For the combined approach, CO₂ emissions of 2.7 (^{3.6}/_{0.5}) Tg y⁻¹ for 2014 and 2.0 (^{2.7}/_{0.4})
634 Tg y⁻¹ for 2015 were derived. EDGAR v4.2 for the year 2008 shows the same order of magnitude when
635 limiting to emissions from refineries and transformation. The results of this study are one order of
636 magnitude smaller compared to CDIAC (Carbon Dioxide Information Analysis Center), Doumbia et al.
637 (2014) and EIA (Energy Information Administration). This emission underestimation is not caused by
638 an underestimation of the flared gas volume. VNF_{flare} includes an estimation of the annual sum of
639 flared gas by country. For Nigeria the estimated values are 8.56 (7.64) bcm flared gas in 2014 (2015).
640 Within this study higher values of 37.89 (20.68) bcm for 2014 (2015) are derived.
641 The deviations might be caused by the uncertainty in the efficiency of the flares concerning the
642 combustion process and their operation. A lack of information regarding the combustion efficiency
643 together with the high sensitivity of the parameters within the combustion equations of IU14 can
644 lead to high uncertainties. Additionally, the usage of emission factors in the existing inventories
645 which did not take into account the spatiotemporal variability of flaring, inconsistent emission sector
646 definitions or the time lag of the emission inventories of 2-5 years can cause deviations. The positive
647 trend in Nigerian gas flaring CO₂ emissions derived by EIA from 38.81 to 52.83 Tg y⁻¹ between 2010
648 and 2013 contradicts the findings of Doumbia et al. (2014) and this study, which generally show a
649 decrease in emissions from 1994 to 2010 and from 2014 to 2015, respectively. Based on the
650 sensitivity study, which reveals high uncertainties of the flaring emission, we conclude that there is
651 no preference in the choice of the climatological and or the combined approach presented in this
652 study. Therefore for simplicity we recommend the use of the climatological approach when using the
653 R package.

654 Despite the generally large uncertainties in the estimation of emissions from gas flaring, this method
655 allows a flexible creation of flaring emission datasets for various applications (e.g. as emission
656 inventory for atmospheric models). It combines observations with physical based background
657 concerning the combustion. The use of current data makes it possible to consider present trends in
658 gas flaring. Even the creation of near real-time datasets with a time lag of one day is possible. The
659 emissions are merged on grid predefined by the user and depending on the availability of VNF data,
660 the temporal resolution can be selected from single days to years.

661 An improvement of this parameterization can be achieved by an extension of the IU14 method to
662 black carbon and VOCs and an inclusion of spatial resolved measurements of the natural gas
663 composition in combination with information of the gas flaring processes from the oil producing
664 industry. Gas flaring is just one of the sources of air pollution in SWA and therefore the DACCIWA
665 field campaign in June-July flaring cannot solely focus on flaring. To provide detailed measurements
666 of the flaring characteristics would go beyond the scope of DACCIWA. However, within the DACCIWA
667 aircraft campaign, the EUFAR (European Facility for Airborne Research) mission APSOWA
668 (Atmosphere Pollution from Shipping and Oil platforms in West Africa) was conducted to
669 characterize gaseous and particulate pollutants emitted by shipping and oil and gas extraction
670 platforms off the coast of West Africa. The authors hope that the results of APSOWA bring further
671 insight in the characteristics of gas flaring in SWA.

672
673

674 **Acknowledgments**

675
676 The research leading to these results has received funding from the European Union 7th Framework
677 Programme (FP7/2007-2013) under Grant Agreement no. 603502 (EU project DACCIWA: Dynamics-
678 aerosol-chemistry-cloud interactions in West Africa). We thank Mikhail Zhizhin from Earth
679 Observation Group (EOG) of NOAA for providing us with the extracted flaring information from the
680 VNF product. We are grateful to Godsgift Ezaina Umukoro (Department of Mechanical Engineering,
681 University of Ibadan, Nigeria) for the kind support during the implementation of their combustion
682 reaction theory into our parameterization.

683

684 **Code and/or data availability**

685
686 This publication includes a package of well documented R scripts which is free available for research
687 purposes and enables the reader to create their own gas flaring emission datasets. It includes
688 exemplarily the preprocessing for June/July 2015 with a focus on southern West Africa. You get
689 access to the code via zenodo.org (DOI: 10.5281/zenodo.61151), entitled “Gas flaring emission
690 estimation parameterization v2”.

691

692 **References**

- 693
694 API, 2007: **Pressure-relieving and Depressuring Systems**, ANSI/API STANDARD 521 FIFTH EDITION,
695 JANUARY 2007, ISO 23251 (Identical), Petroleum and natural gas industries – Pressure-relieving and
696 depressuring systems, American Petroleum Institute, Section 7.3.2.4: Design details h), 127
697
698 Bader, A., Baukal, C. E., Bussman, W. Zink, J., 2011: **Selecting the proper flare systems**, American
699 Institute of Chemical Engineers (AIChE), <http://people.clarkson.edu/wwilcox/Design/FlareSel.pdf>,
700 accessed: October 2, 2014
701
702 CDIAC, 2015a: **Global CO₂ Emissions from Fossil-Fuel Burning, Cement Manufacture, and gas**
703 **Flaring: 1751-2008**, Carbon Dioxide Information Analysis Center (CDIAC),
704 http://cdiac.ornl.gov/ftp/ndp030/global.1751_2008.ems, accessed: December 6, 2015
705
706 CDIAC, 2015b: **National CO₂ Emissions from Fossil-Fuel Burning, Cement Manufacture, and gas**
707 **Flaring: 1751-2011**, Carbon Dioxide Information Analysis Center (CDIAC), Fossil-Fuel CO₂ Emissions by
708 Nation, http://cdiac.ornl.gov/ftp/ndp030/nation.1751_2011.ems, accessed: December 3, 2015
709
710 CM SAF, 2015: **Operational Products: CFC – Fractional cloud cover instantaneous data** (MSG disk,
711 CM SAF definition), Version 350;
712 [https://wui.cmsaf.eu/safira/action/viewPeriodEntry?id=11495_14063_15657_15672_16574_19152_](https://wui.cmsaf.eu/safira/action/viewPeriodEntry?id=11495_14063_15657_15672_16574_19152_20532_21207)
713 [20532_21207](https://wui.cmsaf.eu/safira/action/viewPeriodEntry?id=11495_14063_15657_15672_16574_19152_20532_21207), accessed: November 25, 2015
714
715 Doumbia, T., Granier, L., Liousse, C., Granier, C., Rosset, R., Oda, T., Fen Chi, H., 2014: **Analysis of fifty**
716 **year Gas flaring Emissions from oil/gas companies in Africa**, AGU Fall Meeting 2014, Dec 2014, San
717 Francisco, United States. A13E-3217
718
719 Dung, E. J., Bombom, L. S., Agusomu, T. D., 2008: **The effects of gas flaring on crops in the Niger**
720 **Delta, Nigeria**, *GeoJournal*, Vol., 73, 297-305
721
722 Ekpoh, I. J., Obia, A. E., 2010: **The role of gas flaring in the rapid corrosion of zinc roofs in the Niger**
723 **Delta Region of Nigeria**, *Environmentalist*, Vol. 30, 347-352
724

725 ECCAD, 2015: **Emissions of atmospheric compounds & compilation of ancillary data (ECCAD)**,
726 http://eccad.sedoo.fr/eccad_extract_interface/JSF/page_critere.jsf, accessed: December 4, 2015
727
728

729 EDGAR, 2016: **Global Emissions EDGAR v4.3.2**, European Commission, Joint Research Centre
730 (JRC)/PBL Netherlands Environmental Assessment Agency. Emission Database for Global Atmospheric
731 Research (EDGAR), release version 4.3.2. <http://edgar.jrc.ec.europa.eu>
732

733 EDGAR, 2014: **Global Emissions EDGAR v4.3 FT2012**, European Commission, Joint Research Centre
734 (JRC)/PBL Netherlands Environmental Assessment Agency. Emission Database for Global Atmospheric
735 Research (EDGAR), release version 4.3. <http://edgar.jrc.ec.europa.eu>, 2015 forthcoming,
736 <http://edgar.jrc.ec.europa.eu/overview.php?v=CO2ts1990-2014>, accessed: December 3, 2015
737

738 EIA, 2015: **CO2 from the Consumption and Flaring of Natural Gas**, International Energy Statistics,
739 U.S. Energy Information Administration (EIA),
740 <http://www.eia.gov/cfapps/ipdbproject/iedindex3.cfm?tid=90&pid=3&aid=8&cid=&syid=2010&eyid=2013&unit=MMTCD>, accessed: December 3, 2015
741
742

743 Elvidge, C. D., Zhizhin, M., Baugh, K., Hsu, F.-C., Gosh, T., 2015: Methods for Global Survey of Natural
744 Gas Flaring from Visible Infrared Imaging Radiometer Suite Data, *Energies* 2016, 9, 14, 1-15
745

746 Elvidge, C. D., Zhizhin, M., Hsu, F.-C., Baugh, K. E., 2013: **VIIRS Nightfire: Satellite Pyrometry at Night**,
747 *Remote Sens.*, Vol. 5, 4423-4449
748

749 Elvidge, C. D., Ziskin, D., Baugh, K. E., Tuttle, B. T., Gosh, T., Pack, D. W., Erwin, E. H., Zhizhin, M.,
750 2009: **A fifteen year record of global natural gas flaring derived from satellite data**, *Energies*, Vol. 2,
751 595-622
752

753 Elvidge, C. D., Baugh K. E., Kihn, E. A., Kroehl, H. W., Davis, E. R., 1997: **Mapping city lights with
754 nighttime data from the DMSP operation linescan system**, *Photogrammetric Engineering & Remote
755 Sensing*, Vol. 63, No. 6, 727-744
756

757 EPA, 1985: **Evaluation of the efficiency of industrial flares: Flare head design and gas composition**,
758 Research and Development, United States Environmental Protection Agency (EPA), EPA-600/2-85-
759 106, Tab. 2-6
760

761 Google Earth, 2014: Image 2014 DigitalGlobe, <http://www.earth.google.com>
762

763 Guigard, S. E., Kindzierski, W. B., Harper, N., 2000: **Heat Radiation from Flares**. Report prepared for
764 Science and Technology Branch, Alberta Environment, ISBN 0-7785-1188-X, Edmonton, Alberta.
765

766 Ismail, O. S., Umukoro, G. E., 2014: **Modelling combustion reactions for gas flaring and its resulting
767 emissions**, *Journal of King Saud University – Engineering Sciences*, Vol. 28, 130-140
768

769 Johnson, M. R., Devillers, R. W., Thomson, K. A., 2011: **Quantitative Field Measurements of Soot
770 Emission from Large Gas Flare using Sky-LOSA**, *Environ. Sci. Technol.*, Vol. 45, 345-350
771

772 Knippertz, P., Evans, M. J., Field, P. R., Fink, A. H., Liousse, C., Marsham, J. H., 2015: **The possible role
773 of local air pollution in climate change in West Africa**, *Nature Climate Change*, Vol. 5, 815-822
774

775 Mirador, 2016: AIRS/Aqua Level 2 Standard physical retrieval (AIRS+AMSU), Total cloud fraction
776 (CldFrcTot), [mirador.gsfc.nasa.gov/cgi/bin/mirador/presentNavigation.pl?tree=project&
777 Project=AIRS&data](http://mirador.gsfc.nasa.gov/cgi/bin/mirador/presentNavigation.pl?tree=project&Project=AIRS&data), accessed: April 18, 2016
778

779 NASA, 2016: <http://npp.gsfc.nasa.gov/viirs.html>, accessed: January 5, 2016

780
781 Nwankwo, C. N., Ogagarue, D., O., 2011: **Effects of gas flaring on surface and ground waters in Delta**
782 **State Nigeria**, Journal of Geology and Mining Research, Vol. 3, 131-136
783
784 Nwaugo, V. O., Onyeagba, R. A., Nwahcukwu, N. C., 2006: **Effect of gas flaring on soil microbial**
785 **spectrum in parts of Niger Delta area of southern Nigeria**, African Journal of Biotechnology, Vol. 5,
786 1824-1826
787
788 Osuji, L. C., Awwiri, G. O., 2005: **Flared Gas and Other Pollutants Associated with Air quality in**
789 **industrial Areas of Nigeria: An Overview**, Chemistry & Biodiversity, Vol. 2, 1277-1289
790
791 R Core Team, 2013: **R: A Language and Environment for Statistical Computing**, R Foundation for
792 Statistical Computing, Vienna, Austria, <http://www.R-project.org/>
793
794 Sonibare, J. A., Akeredolu, F. A., 2004: **A theoretical prediction of non-methane gaseous emissions**
795 **from natural gas combustion**, Energy Policy, Vol. 32, 1653-1665
796
797 Strosher, M. T., 2000: **Characterization of Emissions from Diffuse Flare Systems**, Journal of the Air &
798 Waste Management Association, 50:10, 1723-1733
799
800 Strosher, M. T., 1996; **Investigations of flare gas emissions in Alberta**, Final Report to: Environment
801 Canada, Conservation and protection, the Alberta Energy and Utilities Board, and the Canadian
802 Association of Petroleum Producers; Environmental Technologies, Alberta Research Council, Calgary,
803 Alberta
804
805 van der Linden, R., Fink, A. H., Redl, R., 2015: **Satellite-based climatology of low-level continental**
806 **clouds in southern West Africa during the summer monsoon season**, Journal of Geophysical
807 Research: Atmospheres, Vol. 120, 1186-1201
808
809 VDI 3782, 1985: Dispersion of Air Pollutants in the Atmosphere, Determination of Plume rise, Verein
810 Deutscher Ingenieure, VDI-Richtlinien 3782 Part 3, Equation 24, [https://www.vdi.de/richtlinie/
811 vdi_3782_blatt_3-ausbreitung_von_luftverunreinigungen_in_der_atmosphaere_berechnung_der_
812 abgasfahnenueberhoehung/](https://www.vdi.de/richtlinie/vdi_3782_blatt_3-ausbreitung_von_luftverunreinigungen_in_der_atmosphaere_berechnung_der_abgasfahnenueberhoehung/), accessed: October 17, 2016
813
814 VIIRS, 2015a: http://ngdc.noaa.gov/eog/viirs/download_viirs_fire.html, accessed: August 24, 2016
815
816 VIIRS, 2015b: http://ngdc.noaa.gov/eog/viirs/download_viirs_flares_only.html, accessed: July 31,
817 2015
818
819 Vogel, B., Vogel, H., Bäumer, D., Bangert, M., Lundgren, K., Rinke, R., Stanelle, T., 2009: **The**
820 **comprehensive model system COSMO-ART - Radiative impact of aerosol on the state of the**
821 **atmosphere on the regional scale**, Atmos. Chem. Phys., 9, 8661-8680
822
823 World Bank, 2012: [http://www.worldbank.org/content/dam/Worldbank/Programs/Top_20_gas
824 flaring_countries.pdf](http://www.worldbank.org/content/dam/Worldbank/Programs/Top_20_gas_flaring_countries.pdf), accessed: December 5, 2015
825
826 Zhang, X., Scheving, B., Shoghli, B., Zygarlicke, C., Wocken, C., 2015: **Quantifying Gas Flaring CH₄**
827 **Consumption Using VIIRS**, Remote Sens., Vol. 7, 9529-9541
828